Thin Solid Films 548 (2013) 460–464

Contents lists available at ScienceDirect

Thin Solid Films

journal homepage: www.elsevier.com/locate/tsf

Enhancement of the light-scattering ability of Ga-doped ZnO thin films using SiO_x nano-films prepared by atmospheric pressure plasma deposition system

Kow-Ming Chang [a], Po-Ching Ho [a,*], Atthaporn Ariyarit [a], Kuo-Hui Yang [b], Jui-Mei Hsu [b], Chin-Jyi Wu [b], Chia-Chiang Chang [b]

[a] Department of Electronics Engineering & Institute of Electronics, National Chiao Tung University, 1001 Ta Hsueh Road, Hsinchu 30010, Taiwan, ROC
[b] Industrial Technology Research Institute, Mechanical and Systems Research Laboratories, Hsinchu 31040, Taiwan, ROC

ARTICLE INFO

Article history:
Received 22 November 2012
Received in revised form 24 September 2013
Accepted 25 September 2013
Available online 2 October 2013

Keywords:
Transparent conductive oxide
Light-trapping effect
Atmospheric pressure plasma

ABSTRACT

To enhance the light-trapping qualities of silicon thin-film solar cells, the use of transparent conductive oxide with high haze and high conductivity is essential. This study investigated an eco-friendly technique that used bi-layer Ga-doped zinc oxide/SiO_x films prepared with an atmospheric pressure plasma jet to achieve high haze and low resistivity. A minimum resistivity of 6.00×10^{-4} Ω·cm was achieved at 8 at.% gallium doping. Examination of X-ray diffraction spectra showed that increased film thickness led to increased carrier concentration in GZO bilayers. The optimal bilayer GZO film achieved considerably higher haze values in the visible and NIR regions, compared with Asahi U-type fluorine doped tin oxide.

1. Introduction

Transparent conductive oxide (TCO) has attracted substantial attention because of the wide range of its applications. These include solar cells [1–3], flat-panel displays, and light emitting diodes. Two important absorber materials inside silicon thin-film solar cells are amorphous silicon (a-Si) and microcrystalline silicon (μc-Si), both in the form of thin films. To reduce light-induced degradation, the a-Si thin film should be deposited as thinly as possible. By contrast, μc-Si is an indirect semiconductor with a low absorption coefficient, and the μc-Si thin-film should be deposited thickly enough to completely absorb sunlight in a single path. To fulfill these requirements, TCO coatings with properties of high haze and high conductivity should be developed to enhance optical absorption in trapped light [4–7].

A simple technique can be used to produce high haze and high conductivity TCO films. This study developed TCO films using an atmospheric pressure plasma jet (APPJ). The properties of TCO films were compared with those of Asahi U-type TCO glass. The atmospheric pressure chemical vapor deposition (APCVD) process of commercial Asahi U-type fluorine doped tin oxide (FTO) glass requires a high deposition temperature and the use of expensive and toxic gas. Our method used eco-friendly precursors and a low deposition temperature. In addition, the APPJ deposition system offers the advantages of low cost, low temperature processes, and applicability to large substrate processing [8]. The influence of physical properties of SiO_x on the growth of Ga-doped zinc oxide (GZO) films was investigated, and the results showed that the SiO_x buffer layers played an important role in improving the light scattering ability of GZO films.

2. Experiment

Fig. 1 shows a schematic diagram of the experimental apparatus for constructing SiO_x and GZO films, and the route of scan. Silicon suboxide films were deposited on a 5×5 cm^2 alkali-free glass sheet (Asahi, AN100) and scanned over an area of 81 cm^2 by APPJ. The plasma jet was stationary and the substrate was put on the x–y movable stage. The pitch controlled the uniformity of the deposited thin films and the optimal value was 2 mm, as shown in Fig. 1c. The scan speed of y direction was 250 mm/s. Hexamethyl-disiloxane [$(CH_3)_3$-Si-O-Si-$(CH_3)_3$, Alfa Aesar], was used as the precursor and argon was used as the carrier gas to deposit SiO_x thin films on glass substrates at 75 °C. The flow rate of compressed dry air main gas was fixed at 40 SLM. To investigate the influence of the flow rate of argon carrier gas on SiO_x buffer layers, the flow rate was set to vary at 0 sccm, 30 sccm, or 60 sccm. The plasma was generated by applying AC power at 20 kHz. The distance between plasma jet and substrate was 15 mm. GZO films were deposited on SiO_x-coated glass at 150 °C using zinc nitrate ($Zn(NO_3)_2$, 99% purity, J.T.Baker) and gallium nitrate ($Ga(NO_3)_3$, 99.9% purity, Alfa Aesar) as precursors for Zn and Ga ions, respectively. The concentration of zinc nitrate dissolved in deionized water was 0.2 M and the atomic

* Corresponding author.
E-mail address: raymondsam.ee98g@nctu.edu.tw (P.-C. Ho).

0040-6090/$ – see front matter © 2013 Elsevier B.V. All rights reserved.
http://dx.doi.org/10.1016/j.tsf.2013.09.082

percentage of Ga/(Ga + Zn) was set to vary at 6 at.%, 8 at.%, or 10 at.%. The precursor solution was ultrasonically atomized at 2.45 MHz into mist and then carried by nitrogen gas through the plasma-discharging area. The plasma was generated with a 15 kV DC pulse, which has repetition rate of 25 kHz. The plasma power of the DC pulse power supply was fixed at 625 W (Input voltage: 250 V; Current: 2.5 A). The flow rate of N_2 main gas and N_2 carrier gas was 35 SLM and 300 sccm, respectively. The scan speed of x was 50 mm/s and the scan speed of y was 20 mm/s. The pitch was fixed at 2 mm. The deposition time of APPJ was set to vary at 16, 24, or 32 min to obtain the optimal thickness of GZO film.

The surface morphology and thickness of SiO_x buffer layers and GZO films were analyzed using a scanning electron microscope (SEM; Hitachi, S-4700I) with 15 kV operating voltage. The surface elemental composition of the SiO_x thin films was measured using X-ray photoelectron spectroscopy (XPS; ULVAC-PHI, PHI 1600). The binding energy scale of each element was calibrated to 285.43 eV (C1s). Auger electron spectroscopy (AES; ULVAC-PHI, PHI 700) was performed to determine the atomic percentage of gallium in the films. The sample was ion-etched by argon sputtering for 2 min to remove surface contamination (acceleration voltage of 5 kV) before XPS and AES investigation. The roughness was determined by atomic force microscopy (AFM; Digital Instruments, D3000) with high aspect ratio tips (NANOSENSORS, AR5-NCHR-20) for tapping mode. Electrical properties of GZO films were analyzed by Hall measurement (ACCENT, HL5500PC). The optical transmittance and haze values were measured using an UV–vis–NIR spectrophotometer (Jasco, V570). X-ray diffraction spectra of bilayer GZO films were measured using an X-ray diffractometer (XRD; Bruker, D8 Advance) with CuKα (λ = 1.54 Å) radiation source in Bragg–Brentano geometry.

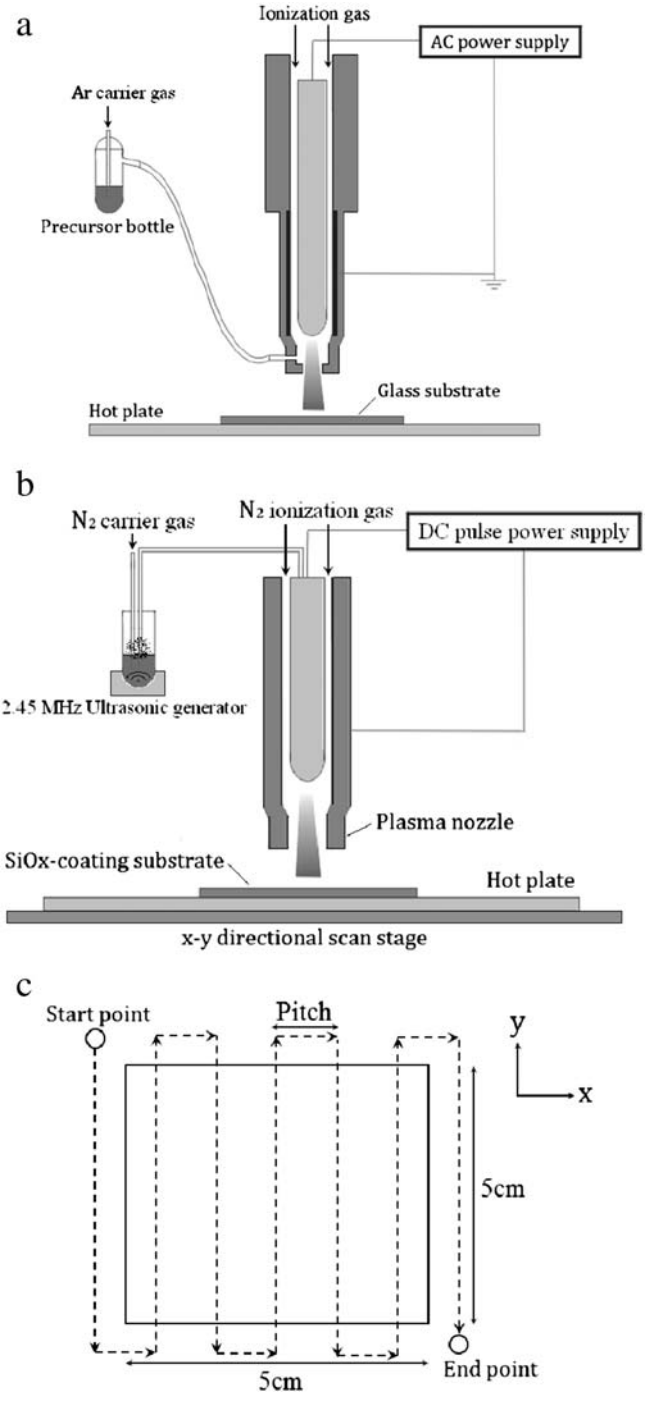

Fig. 1. Schematic diagram of the experimental equipment for (a) SiO_x and (b) GZO; and (c) the scan path.

3. Results and discussion

3.1. SiO_x buffer layer effect

The APPJ was used to deposit rough morphology of SiO_x [9] by changing the distance between nozzle and substrate, substrate temperature and carrier gas flow rate. Preliminary experiments showed that carrier gas flow rate can precisely control the thickness and roughness of SiO_x thin films. Based on this result, SiO_x thin films were deposited at argon carrier gas flow rates of 30 sccm and 60 sccm. Fig. 2a and b shows the cross-sectional and surface SEM images of SiO_x buffer layers deposited at an argon carrier gas flow rate of 30 sccm. It can be seen that the surface was rough and contains particles. At 30 sccm and 60 sccm, the root mean square (RMS) roughness of SiO_x thin films was 12.20 nm and 34.87 nm. The thickness of sample of 30 sccm (60 sccm) ranged from 21.0 nm (36.2 nm) to 102 nm (242.9 nm). The elemental composition of SiO_x films measured by XPS showed that the atomic concentration of C1s, O1s and Si2p3 was 10.04 at.%, 59.48 at.% and 30.48 at.%, respectively. The O/Si atomic ratio was 1.95 and it revealed that oxidization was not fully promoted. The presence of carbon in the SiO_x buffer layer was attributed to Si-$(CH_3)_x$ groups produced by the reaction of silicon with methyl groups [10]. The main difference between vacuum and non-vacuum deposition techniques is the mean free path (MFP) of radicals, which is associated with working pressure. The formation of rough surface of SiO_x was due to short MFP and successive collisions between radicals inside plasma nozzle. The surface roughness of an SiO_x buffer layer is known to influence the optical properties of GZO films subsequently deposited [10,11]. Fig. 2c and d shows cross-sectional SEM images of GZO/SiO_x bilayers and magnified images around the GZO/SiO_x interface. It was found that the grain size of GZO thin film increased vertically because of rough surface of SiO_x buffer layers. The radicals generated by APPJ have low migration on the rough SiO_x surface, which resulted in decreasing of nuclei density. After formation of critical size nuclei, small island formed subsequently on the SiO_x surface. As growth proceeds, the island was difficult to contact with the other island edges because of few nucleation sites on SiO_x surface. Finally, this resulted in V-shaped GZO grain due to difference of growth rate in vertical and horizontal direction.

Fig. 3 shows the transmittance and haze spectra of conventional GZO films and bilayer GZO films deposited on various SiO_x buffer layers. Silicon suboxide thin films were deposited at argon carrier gas flow rates of 30 sccm and 60 sccm. As the surface roughness increased, the transmittance of bilayer GZO films has a slight decrease in visible region (Fig. 3a). It is noteworthy that interference fringes of the sample of 60 sccm almost disappear. A possible explanation for this is that the rough morphology of bilayer GZO reduced the interference of light. As shown in Fig. 3b, the haze values of bilayer GZO films in the visible region were significantly increased, compared with conventional GZO films (without SiO_x buffer layers). This result implies that bilayer GZO

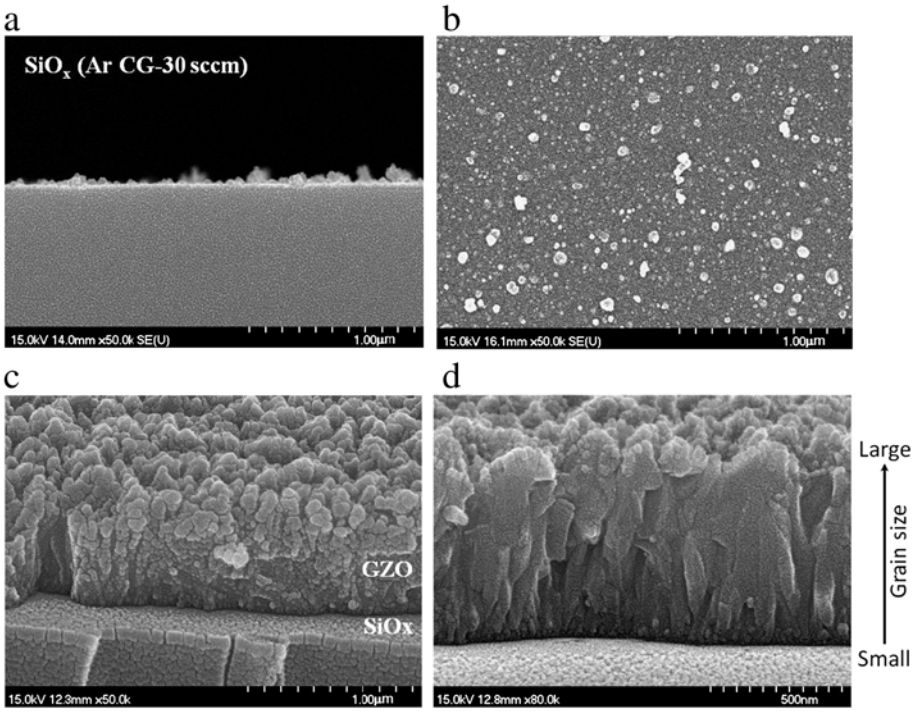

Fig. 2. SEM images of (a, b) SiO_x buffer layers and (c) GZO/SiO_x bilayers; and (d) magnified around the GZO/SiO_x interface.

films display more diffuse transmittance at the surface than do conventional GZO film. Data in Table 1 show the Hall measurement results of conventional GZO and bilayer GZO. The sample of 30 sccm achieved the lowest resistivity and the highest Hall mobility. The sample of 60 sccm has similar electrical properties and higher haze value, but its surface was too rough to deposit thin films in subsequent process. Consequently, the argon carrier gas of 30 sccm was used to deposit SiO_x buffer layers.

3.2. Gallium doping concentration effect

Silicon suboxide thin films were deposited at argon carrier gas flow rates of 30 sccm and then GZO thin films were subsequently deposited on them using various Ga concentration precursors. Fig. 4 shows the resistivity, Hall mobility, and carrier concentration of bilayer GZO films for Ga atomic ratio from 6 at.% to 10 at.%. The minimum mobility of 14.1 $cm^2/V \cdot s$ was measured at 10 at.% gallium doping because of ionized impurity scattering [12]. The minimum resistivity of 6.00×10^{-4} Ω·cm was obtained at approximately 8 at.% gallium doping. A possible explanation for this finding is the efficient occupation of Zn substitutional sites by Ga atoms in the wurtzite structure [13], which results in the highest carrier concentration of 6.58×10^{20} cm^{-3}. The calculated optical band gap in bilayer GZO films for a Ga doping concentration of 6 at.%, 8 at.% and 10 at.% was 3.71 eV, 3.82 eV and 3.74 eV, respectively. According to the Burstein–Moss effect, the optical band gap increases when carrier concentrations exceed the conduction band edge density of states. The relation between broadening of the optical band gap and carrier concentration was estimated using the following formula [14]:

$$\Delta E_{opt} = \left(\frac{\hbar^2}{2m_{cv}^*}\right)\left(3\pi^2 n\right)^{\frac{2}{3}}$$

where is the reduced Planck constant, m_{cv}^* is the reduced effective mass and n is the carrier concentration. The sample of 8 at.% gallium doping had a maximum optical band gap of 3.82 eV and the result was consistent with the Hall measurements of carrier concentrations, as shown in Fig. 4. A decrease in optical band gap was observed at 10 at.%; a possible explanation is that excess dopants might have been trapped at the grain boundaries instead of contributing as free carriers [15]. The optical properties of various Ga concentrations of GZO bilayers are summarized in Table 2. As a result, the sample of 8 at.% has the highest transmittance of 82.2% at the wavelength of 550 nm.

In this study, the Ga content was higher than that reported in literatures (2 at.%–5 at.%) [16–18]. It can be speculated that the gallium doping efficiency of the APPJ was less efficient than that of vacuum deposition techniques, such as magnetron sputtering. This may be due to the difference of working pressure between high vacuum and atmospheric pressure. The sample of 6 at.% has the highest Hall mobility and the lowest carrier concentration, which could reduce absorption of light in near infrared region, however, the larger deviation of its electrical properties indicated that it was non-uniform. Based on the electrical and optical results, the optimal gallium doping concentration was 8 at.%.

3.3. Effect of GZO film thickness

As mentioned above, silicon suboxide buffer layers were deposited at argon carrier gas flow rates of 30 sccm and the optimal Ga/(Ga + Zn) ratio of precursor was 8 at.%. The thickness of GZO bilayers measured by SEM was 450 nm, 630 nm, and 775 nm, respectively, for deposition time of 16, 24, and 32 min. Fig. 5 shows the XRD patterns of bilayer GZO films of varying thickness. The bilayer GZO films exhibited two obvious (002) and (101) diffraction peaks. An increase in film thickness led to an increase in intensity of (002) and (101) peaks, as shown in Fig. 5. The full width at half maximum (FWHM) of (002) main peaks decreased from 0.262 to 0.241° as the thickness of films increased from 450 nm to 775 nm. These results indicated a significant increase in the crystallinity of bilayer GZO films. Notably, the ionic radius of Ga is smaller than that of Zn; thus, gallium incorporation yields a lower lattice constant [19]. A positive correlation was evident between the lattice constant and lattice plane d-spacing, and the Bragg angle was determined from d-spacing. The positive shift in 2theta values of (002) peaks for bilayer GZO films resulted from incremental increases in Ga doping concentration. The atomic percentage of gallium of bilayer GZO films measured by Auger electron spectroscopy was 2.85 at.%,

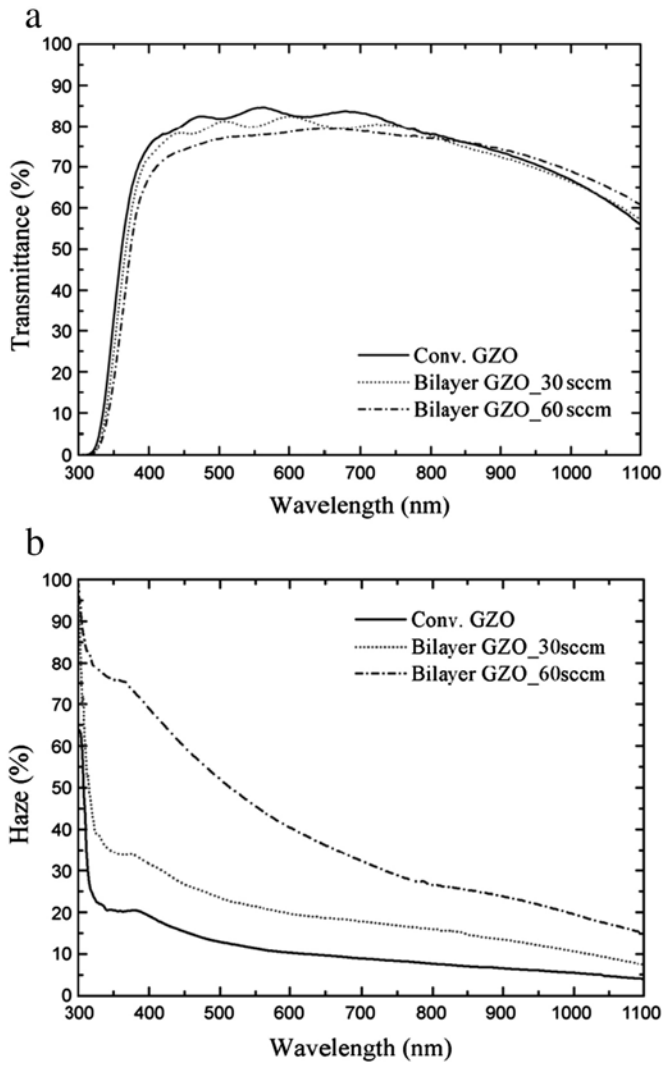

Fig. 3. (a) Transmittance and (b) haze spectra of conventional GZO and bilayer GZO films deposited on SiO_x buffer layers at various carrier flow rates. Conventional GZO and bilayer GZO films were scanned 20 times by APPJ.

2.96 at.%, and 3.25 at.%, respectively, for thickness of 450 nm, 630 nm, and 775 nm. As a result, an increase in crystallinity of GZO bilayers resulted in an increase in Ga at.%.

3.4. Comparison of GZO bilayers and Asahi U-type FTO

Asahi U-type FTO glass is produced by Asahi Glass Company (AGC), and it is used as the front electrode of a-Si solar cells. The process step of Asahi U-type is depositing FTO on glass substrates by using atmospheric pressure chemical vapor deposition (APCVD) and then proceeding wet etching. The biggest drawback of FTO thin film is not applicable to the process of hydrogen rich plasma, such as deposition of hydrogenated microcrystalline silicon (μc-Si:H) thin films for a long time. Because tin

Table 1
Electrical properties of conventional GZO and bilayer GZO.

	Resistivity (Ω·cm)	Hall mobility ($cm^2 V^{-1} s^{-1}$)	Carrier concentration (cm^{-3})
Conventional GZO	6.19×10^{-4}	10.6	9.74×10^{20}
Bilayer GZO_30 sccm	6.00×10^{-4}	15.8	6.58×10^{20}
Bilayer GZO_60 sccm	7.18×10^{-4}	15.2	5.72×10^{20}

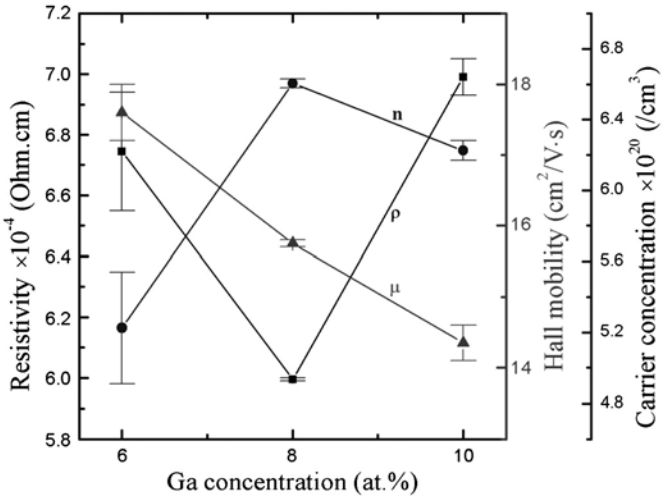

Fig. 4. Resistivity (ρ), Hall mobility (μ), and carrier concentration (n) of bilayer GZO films deposited for various Ga/(Zn + Ga) atomic ratios.

Table 2
Optical (at 550 nm) properties of various Ga concentrations of bilayer GZO films.

	6 at.%	8 at.%	10 at.%
Thickness (nm)	780	775	705
Transmittance (%)	80.90	82.20	80.35
Haze (%)	23.79	21.50	24.40

can be reduced by hydrogen plasma, which results in decreasing of transmittance of FTO. Consequently, it is necessary to deposit a ZnO or TiO_2 capping layer on FTO to protect against hydrogen plasma [20]. Conversely, GZO material has high resistance to resist hydrogen plasma.

Fig. 6 shows the SEM surface images of GZO/SiO_x bilayers and Asahi U-type FTO. Fig. 7 shows a comparison for transmittance and haze between Asahi U-type FTO films and bilayer GZO films with varying thickness. The transmittance in the 750- to 1100-nm region was lower than 80% for all bilayer GZO films, as shown in Fig. 7a; this was attributed to the high carrier concentration increasing the free carrier absorption. The 775-nm-thick bilayer GZO film achieved considerably higher haze values in the visible and NIR regions, compared with Asahi U-type FTO or other bilayer GZO films, as shown in Fig. 7b. Table 3 shows a comparison of Asahi U-type FTO and bilayer GZO films. The optimal bilayer GZO film was 775 nm thick and showed lower resistivity compared with Asahi U-type FTO film. The optimized bilayer GZO film was thinner

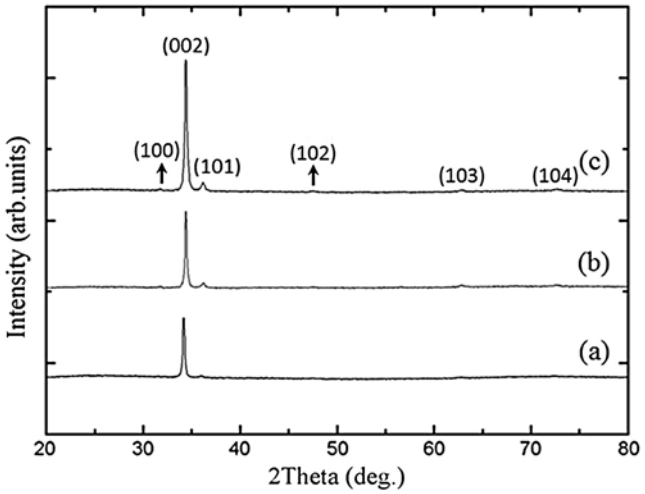

Fig. 5. XRD patterns of bilayer GZO of various thickness: (a) 450 nm; (b) 630 nm; and (c) 780 nm.

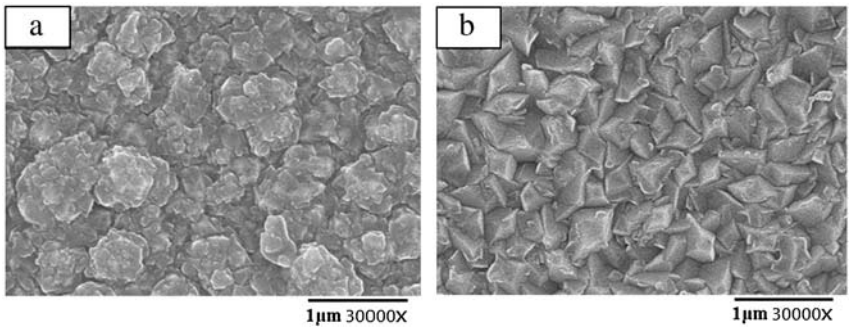

Fig. 6. SEM surface images of (a) GZO/SiO_x bilayers and (b) Asahi U-type FTO.

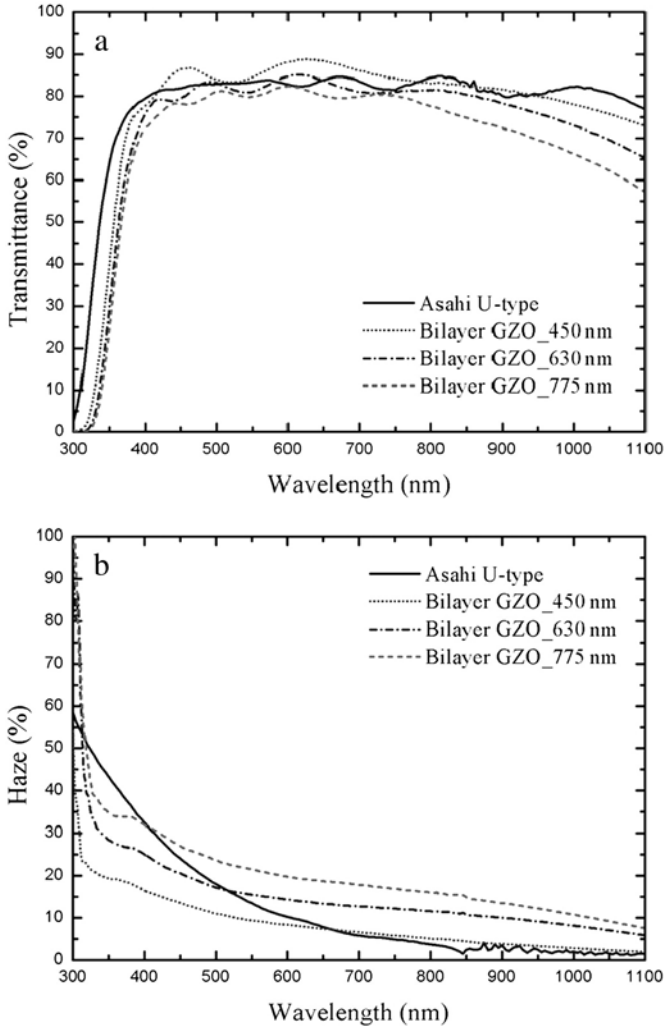

Fig. 7. (a) Transmittance and (b) haze of Asahi U-type FTO film and bilayer GZO films of various thickness: 450 nm, 630 nm and 780 nm.

Table 3
Comparison of bilayer GZO films and Asahi U-type FTO.

	Bilayer GZO	Asahi U-type
Structure	GZO/SiO_x/glass	Textured FTO/glass
Technique	APPECVD	APCVD + etching
Substrate temperature (°C)	140	450
Thickness (nm)	775	900
RMS (nm)	40.73	33.10
Transmittance (%) at 550 nm	82.2	83.0
Haze (%) at 550 nm	21.50	13.50
Resistivity (Ω·cm)	6.00×10^{-4}	7.38×10^{-4}
Hall mobility ($cm^2\ V^{-1}\ s^{-1}$)	15.8	46.2
Carrier concentration (cm^{-3})	6.58×10^{20}	1.83×10^{20}

than Asahi-U type FTO film, but performed similarly. This result suggested that APPJ deposition might entail relatively less material consumption than APCVD deposition.

4. Conclusion

In summary, the bilayer GZO film qualities of high haze and low sheet resistance is achieved by APPJ. The thickness and RMS roughness of SiO_x buffer layers increase as the argon carrier gas flow rates increase. An increase in the roughness of SiO_x buffer layers is associated with a significant increase in the haze values of bilayer GZO films. The minimum resistivity of 6.00×10^{-4} was achieved at 8 at.% gallium doping, which had the highest carrier concentration. An increase in thickness of film led to an increase in intensity of (002) main peaks, Hall mobility, and carrier concentration. The bilayer GZO film was thinner than Asahi-U type FTO film but achieved similar electrical and optical performance. Furthermore, the 775-nm-thick bilayer GZO film had a considerably higher haze value in the visible and NIR regions compared with Asahi U-type FTO film. These results suggest that APPJ is an effective method for preparing textured TCO.

Acknowledgment

The authors are grateful for research support provided by the Mechanical and Systems Research Laboratories, Industrial Technology Research Institute (ITRI).

References

[1] C.H. Huang, H.L. Cheng, W.E. Chang, M.S. Wong, J. Electrochem. Soc. 158 (2011) H510.
[2] B. Sang, K. Kushiya, D. Okumura, O. Yamase, Sol. Energy Mater. Sol. Cells 67 (2001) 237.
[3] E. Fortunato, L. Raniero, L. Silva, A. Gonc-alves, A. Pimentel, P. Barquinha, H. A´guas, L. Pereira, G. Goncalves, I. Ferreira, E. Elangovan, R. Martins, Sol. Energy Mater. Sol. Cells 92 (2008) 1605.
[4] J. Muller, B. Rech, J. Springer, M. Vanecek, Sol. Energy 77 (2004) 917.
[5] M. Kambe, M. Fukawa, N. Taneda, Y. Yoshikawa, K. Sato, K. Ohki, S. Hiza, A. Yamada, M. Konagai, Proceedings of 3rd World Conference on Photovoltaic Energy Conversion, vol. 2, IEEE, Osaka, Japan, 2003, p. 1812.
[6] O. Kluth, B. Rech, L. Houben, S. Wieder, G. Schope, C. Beneking, H. Wagner, A. Loffl, H.W. Schock, Thin Solid Films 351 (1999) 247.
[7] J. Krc, M. Zeman, O. Kluth, F. Smole, M. Topic, Thin Solid Films 426 (2003) 296.
[8] K.M. Chang, S.H. Huang, C.J. Wu, W.L. Lin, W.C. Chen, C.W. Chi, J.W. Lin, C.C. Chang, Thin Solid Films 519 (2011) 5114.
[9] S.H. Yang, C.H. Liu, C.H. Su, H. Chen, Thin Solid Films 517 (2009) 5284.
[10] S.H. Yu, P.C. Ho, T.W. Yang, C.C. Bi, C.H. Yeh, C.Y. Chang, ECS Solid State Lett. 1 (2012) 48.
[11] B.D. Ahn, Y.G. Ko, S.H. Oh, J.H. Song, H.J. Kim, Thin Solid Films 517 (2009) 6414.
[12] H. Makino, Y. Sato, N. Yamamoto, T. Yamamoto, Thin Solid Films 520 (2011) 1407.
[13] D.W. Kang, S.H. Kuk, K.S. Ji, S.W. Ahn, M.K. Han, Jpn. J. Appl. Phys. 49 (2010) 031101.
[14] F. Wu, L. Fang, Y.J. Pan, K. Zhou, Q.L. Huang, C.Y. Kong, Phys. E. 43 (2010) 228.
[15] T. Yamada, H. Makino, N. Yamamoto, T. Yamamoto, J. Appl. Phys. 107 (2010) 123534.
[16] L. Gong, J. Lu, Z. Ye, Sol. Energy Mater. Sol. Cells 94 (2010) 1282.
[17] D.H. Kim, S.H. Lee, G.H. Lee, H.B. Kim, K.H. Kim, Y.G. Lee, T.H. Yu, J. Appl. Phys. 108 (2010) 023520.
[18] H. Akazawa, Thin Solid Films 520 (2011) 2418.
[19] K.T. Ramakrishna Reddy, H. Gopalaswamy, P.J. Reddy, R.W. Miles, J. Cryst. Growth 210 (2000) 516.
[20] J. Poortmans, V. Arkhipov, Thin film solar cells fabrication, Characterization and Applications, Wiley, 2007. 209.